ELSEVIER

Deep-Sea Research II 51 (2004) 43–57

DEEP-SEA RESEARCH
PART II

www.elsevier.com/locate/dsr2

Seasonal patterns of sea-surface temperature and ocean color around the Galápagos: regional and local influences ☆

Daniel M. Palacios*

College of Oceanic and Atmospheric Sciences, Oregon State University, Corvallis, OR 97331-5503, USA

Received 23 April 2003; received in revised form 18 August 2003; accepted 20 August 2003

Abstract

Monthly climatologies of satellite-derived sea-surface temperature (SST, from AVHRR) and ocean color (from Ocean Color and Temperature Scanner and Sea-viewing Wide-Field-of-view Sensor) around the Galápagos Archipelago are used to estimate the mean seasonal cycle of these properties and their relationship to the equatorial circulation in this oceanographically complex region. Harmonic analysis of the climatological time series indicates a best fit with annual and semi-annual constituents. The annual amplitude is the dominant signal in SST, corresponding to the basin-wide seasonal cycle of warming and cooling associated with the north–south migration of the intertropical convergence zone. Influx of upwelled water from the Panamá Bight into the northeastern part of the study area is also consistent with the annual signal. An empirical orthogonal function decomposition identifies two main spatial patterns with amplitude time series representing out-of-phase annual cycles. The dominant mode corresponds to the strengthening of the Equatorial Front and the South Equatorial Current during the second part of the year. This mode explains 92.2% of the SST variance and 82.9% of the ocean-color variance. The second mode is consistent with the topographically induced upwelling of the Equatorial Undercurrent on the western side of the archipelago, and with influx of upwelled Panamá Bight water on the eastern side, both reaching their peak during the first part of the year. This mode accounts for 6% of the SST variance and 7.7% of the ocean-color variance. The seasonal evolution of water-column temperature and nitrate (from World Ocean Atlas 1998 climatologies) is consistent with the satellite-derived patterns. A slight tilt aligned with the east–west axis of the Galápagos Platform (outlined by the 2000-m isobath) is evident in all property fields, suggesting that the presence of the archipelago introduces a small but noticeable perturbation to the large-scale currents and property gradients of the eastern equatorial Pacific.

1. Introduction

Located in the eastern equatorial Pacific, the Galápagos Archipelago lies in an area of rapid change in oceanographic conditions owing to its proximity to the Equatorial Front (EF). The EF is a regional feature that runs zonally between the South American coast and the international date-line, separating warm waters to the north from cool waters to the south. Biological production across this gradient is strongly influenced by the availability of macronutrients (i.e. nitrate) and micronutrients (i.e. iron). Conditions are generally oligotrophic north of the EF due to a meager

☆ Supplementary data associated with this article can be found, in the online version, at doi: 10.1016/j.dsr2.2003.08.001.

*Current address: NOAA/NMFS/Pacific Fisheries Environmental Laboratory, 1352 Lighthouse Avenue, Pacific Grove, CA 93940-2097, USA. Fax: +1-831-648-8440.

E-mail address: dpalacios@pfeg.noaa.gov (D.M. Palacios).

0967-0645/$ - see front matter © 2004 Elsevier Ltd. All rights reserved.
doi:10.1016/j.dsr2.2003.08.001

nitrate supply across the strong pycnocline. South of the EF, wind-induced equatorial upwelling provides nitrate in adequate concentrations, but iron is in limited supply, leading to "high-nutrient, low-chlorophyll" (HNLC) conditions through most of this region. Only at the Galápagos is this condition relieved owing to a localized phenomenon, the topographically forced upwelling of the Equatorial Undercurrent (EUC) on the western side of the archipelago. In this area, phytoplankton populations are able to use the upwelled nitrate in the presence of a local source of iron derived from the island platform (Gordon et al., 1998; Lindley and Barber, 1998). The productive habitat that develops in this area can be seen in ocean-color satellite imagery as a plume of elevated phytoplankton pigment concentration extending westward for 100 km or more (Feldman et al., 1984; Feldman, 1986; Palacios, 2002). Thus, within Galápagos waters it is possible to find warm/oligotrophic, cool/HNLC, and cool/eutrophic conditions in close proximity to each other.

This static description does not consider the seasonal cycle, which is a major signal in the eastern equatorial Pacific (e.g. Hayes, 1985; Delcroix, 1993; Yu and McPhaden, 1999; Johnson et al., 2002). It has been known for some time that despite lying on the equator, the annual cycle of sea-surface temperature (SST) at the Galápagos follows a distinct southern hemisphere schedule (Abbott, 1966). However, this observation is based on localized measurements from shore stations in the central part of the archipelago, and it has been suggested that the northern sector may be under a different regime (Harris, 1969). Also puzzling is the apparent lack of seasonality in phytoplankton abundance despite the clear SST cycle (Harris, 1969; Houvenaghel, 1978, 1984; Kogelschatz et al., 1985; Feldman, 1986).

Monthly climatologies of remotely sensed SST and ocean color (i.e. the concentration of near-surface phytoplankton chlorophyll *a*) are used in this paper to estimate the mean seasonal cycle of these properties for the Galápagos region. The islands lie at the confluence of several current systems, as illustrated in Fig. 1. The degree of exposure of the different sectors of the archipelago

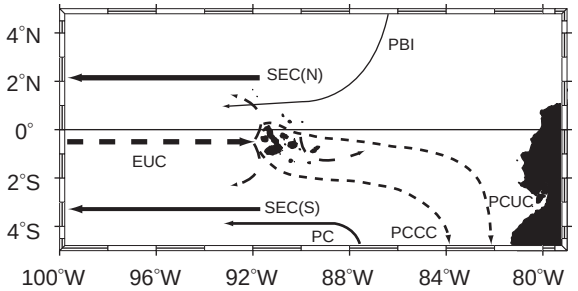

Fig. 1. Schematic representation of the current systems in the vicinity of the Galápagos Islands. SEC = South Equatorial Current, EUC = Equatorial Undercurrent, PBI = Panamá Bight Influence, PC = Perú Current, PCCC = Perú–Chile Countercurrent, PCUC = Perú–Chile Undercurrent. Dashed arrows represent subsurface flows. Adapted from Pak and Zaneveld (1973), Anderson (1977), Lukas (1986), and Strub et al. (1998).

to the currents, as well as the interaction of these flows with the underwater topography, undoubtedly have important effects. Consequently, an additional goal of this paper is to describe the effects of the presence of the archipelago on these flows, as manifested in the satellite fields.

2. Study area

The area for this study is defined as a $7 \times 7^\circ$ latitude–longitude box extending from 3°N to 4°S and from 87 to 94°W, and encompassing all environment types found around the Galápagos, as described in the introduction. The spatial extent of the area thus defined is about 605×10^3 or $597 \times 10^3\,\mathrm{km}^2$ if the area of the islands is subtracted (Fig. 2).

3. Satellite climatologies

Climatological monthly fields of satellite-derived SST and ocean color (chlorophyll-*a* concentration, or chl) with a spatial resolution of 9.28 km are used here to investigate patterns of spatial and temporal variability around the Galápagos Islands. The SST climatologies are a standard product known as the "Pathfinder + Erosion" monthly climatologies, distributed by the Physical

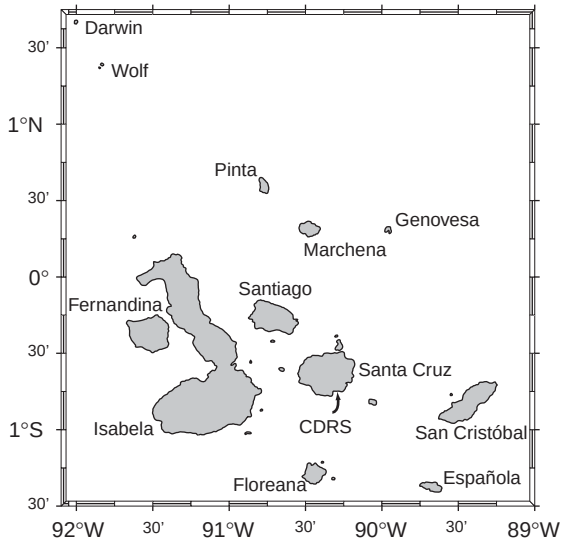

Fig. 2. Map of the Galápagos Archipelago with the names of the main islands. The arrow indicates the location of the CDRS dock.

Oceanography Distributed Active Archive Center (PO.DAAC) at the Jet Propulsion Laboratory (JPL) of the California Institute of Technology and the National Aeronautics and Space Administration (NASA). This product was computed from a 13-year period (1985–1997) of Advanced Very High Radiometer (AVHRR) measurements processed with versions 4.0 and 4.1 of the Pathfinder Oceans algorithm. Casey and Cornillon (1999) describe the production of these climatologies through 1995. Briefly, daily fields (daytime and nighttime passes of the satellite) were averaged into monthly time series after applying an "erosion filter" near cloud-flagged pixels that further reduced the possibility of cloud contamination. For each month of the year, all data corresponding to that month in the 1985–1997 series were averaged, resulting in an initial climatology consisting of 12 monthly means. Although the global mean fields were essentially complete, small gaps with no data remained in regions with persistent cloud clover. These gaps were filled with the median value of the surrounding SST values from the 7×7 pixel box ($\sim 65 \times 65$ km) centered on the missing pixel. Only few pixels were missing after the first median filter, and these were interpolated with a second 11×11 ($\sim 102 \times 102$ km) median filter, effectively removing all remaining gaps, but leaving the non-missing pixels unchanged. Finally, small-scale noise was removed with a 7×7 median smoother applied to each entire field (Casey and Cornillon, 1999).

Ocean-color climatologies were formed for the 6.7-year period November 1996–June 2003 by combining chl concentrations derived from two sensors: the Ocean Color and Temperature Scanner (OCTS), which operated between November 1996 and June 1997, and the Sea-viewing Wide-Field-of-view Sensor (SeaWiFS), which has been in operation since September 1997. These data are produced by the SIMBIOS-NASDA-OCTS and the SeaWiFS projects at the NASA Goddard Space Flight Center (GSFC) and distributed by the GSFC Earth Sciences Data and Information Services Center Distributed Active Archive Center (GES DISC DAAC). The monthly ocean-color products at 9.28-km resolution for the OCTS and SeaWiFS sensors were initially combined into an ocean-color time series that contained data for the 80-month period November 1996–June 2003. There was a 2-month gap between the two missions in July and August 1997 for which there were no data. The same procedure used by Casey and Cornillon (1999) to produce the monthly SST climatologies was applied to the ocean-color time series, except that the fields were not eroded. Since chl values spanned three orders of magnitude, the ocean-color data were log-transformed prior to analysis in order to homogenize the variance. An animated sequence of the final 12 monthly climatologies is included online (Animation 1).

4. Harmonic analysis

Harmonic analysis (Emery and Thomson, 1997) was applied to the SST and ocean-color monthly climatologies to investigate their fit to a seasonal cycle composed of an annual and a semi-annual period. Phase lags are given in months relative to 15 January, the first month in the time series.

Fig. 3 shows the mean fields computed from the 12 SST and ocean-color monthly climatologies. It

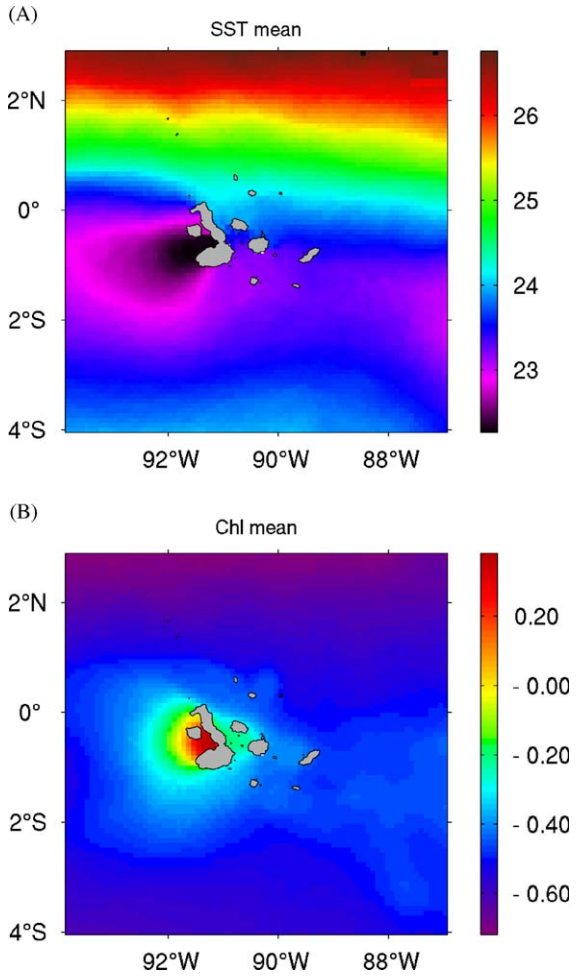

Fig. 3. Temporal mean fields of "Pathfinder + Erosion" SST (°C) (A); and log-transformed OCTS/SeaWiFS chl ($mg\,m^{-3}$) (B) monthly climatologies, respectively.

is apparent that the archipelago lies within a region with a strong north–south thermal gradient. The EF, a band where the most rapid changes take place (i.e. the 24–26°C interval) is located between 1°N and 2°N on the western side of the study area and between 0°N and 1°N on the eastern side (Fig. 3A). The principal effect of the presence of the island platform in the region is to block the EUC (see Fig. 1), forcing some of its waters to upwell and form a pool of cold water on the western side of the archipelago (Fig. 3A). Phytoplankton populations in this pool are enhanced, according to the very high chl concentrations observed in Fig. 3B. A zonal band of cool water (and somewhat elevated chl levels) extends eastward from this pool, mainly along the southern margin of the archipelago, possibly marking the path of the shallow southern branch of the EUC as it continues its journey toward the South American continent (see Fig. 1).

Fig. 4 shows the annual and semi-annual amplitudes, together with the percent of the variance explained by the fit. The harmonic fit explains a large percentage of monthly variability for both SST and chl throughout much of the study area (R^2 range: 85.3–99.9% for SST; 17–96.7% for chl) (Figs. 4E and F). The SST annual amplitude (Fig. 4A) is the dominant signal. It represents a large-scale pattern of warming and cooling that is most evident in the southern half of the study area. On the other hand, the semi-annual amplitude (Fig. 4C) is small throughout the study area (<0.9°C), and only becomes important in localized areas along the northern sector. Although the chl annual amplitude also represents a regional pattern with large excursions at the southeast corner of study area (Fig. 4B), the plume of enhanced phytoplankton on the western side of the archipelago shows the greatest variability. The magnitude of the semi-annual constituent is about as large as that of the annual amplitude in this area, suggesting that the plume is highly variable on an intraseasonal scale as well.

One particularly interesting feature in the annual amplitude, most noticeable in the SST field, is a southward tilt in the pattern of about 1.5° in latitude from west to east that is aligned with the shape of the archipelago (as indicated by the 2000-m depth contour in Fig. 4A). This feature is best explained in terms of the annual phase (Fig. 5A), which indicates that much of the study area reaches maximum temperatures around March, when the southeast trade winds that normally cool the region are weakest and the intertropical convergence zone (ITCZ) is at its southernmost position. However, a distinct wedge-shaped area on the eastern sector reaches its maximum temperature about 2 months earlier. At that time the area begins receiving the influx of upwelled waters from the Panamá Bight (Cromwell and Bennett, 1959; Wooster, 1959). It appears

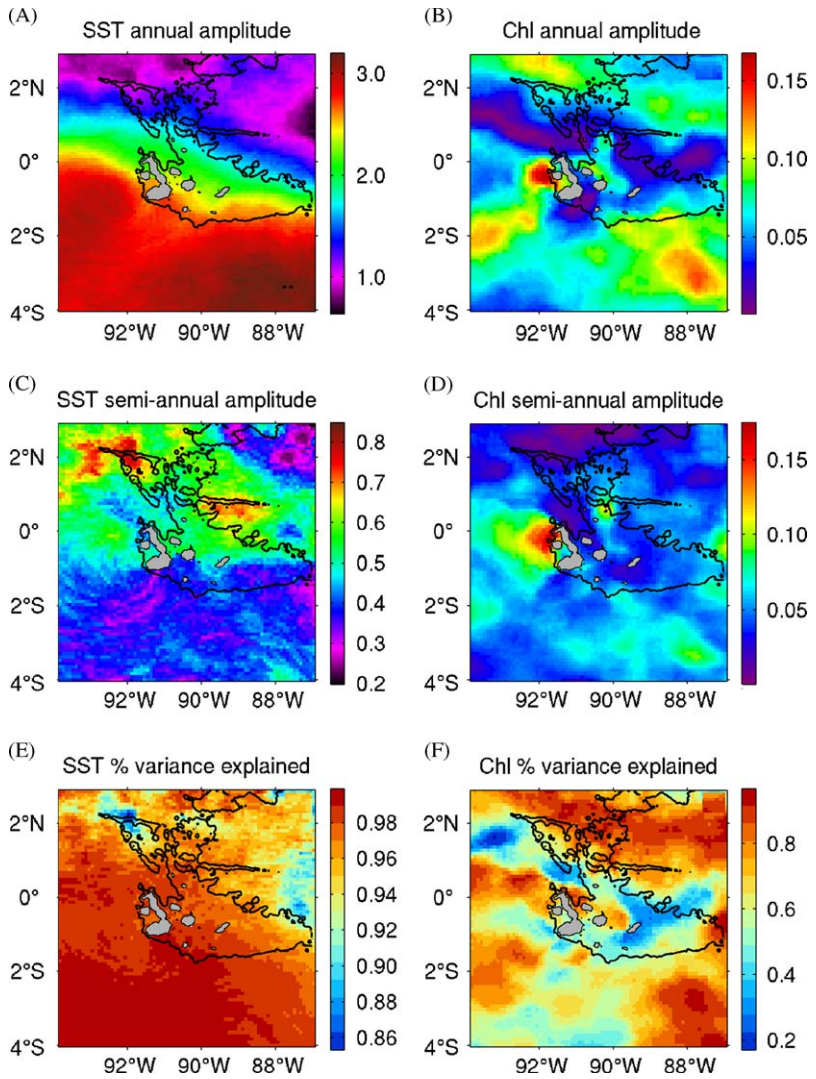

Fig. 4. Harmonic analysis: (A,B) annual amplitude constituents for SST (°C) and log-transformed chl ($mg\,m^{-3}$), respectively; (C,D) semi-annual amplitude constituents for the same variables; and (E,F) percent explained variance by the harmonic fit for the same variables. Black contour indicates the 2000-m isobath.

that the islands act as an obstacle to the penetration of these waters, as the annual phase is locked-in with the shape of the archipelago (indicated by the 2000-m depth contour in Fig. 5A) in this sector. This phenomenon also explains the tilt in the amplitude pattern: the influx of cool waters prevents this sector from reaching maximum temperatures during this period.

The chl annual phase (Fig. 5B) reveals two distinct annual cycles within the study area, one peaking in the austral fall (around May) in the northern part and the other one peaking in the austral spring (around August) in the southern part. The northern cycle is consistent with the annual advection of waters enriched with phytoplankton (or possibly colored dissolved organic matter) from the Panamá Bight, while the southern cycle represents the increase in phytoplankton biomass resulting from equatorial upwelling during the southeast trade wind season. The phase

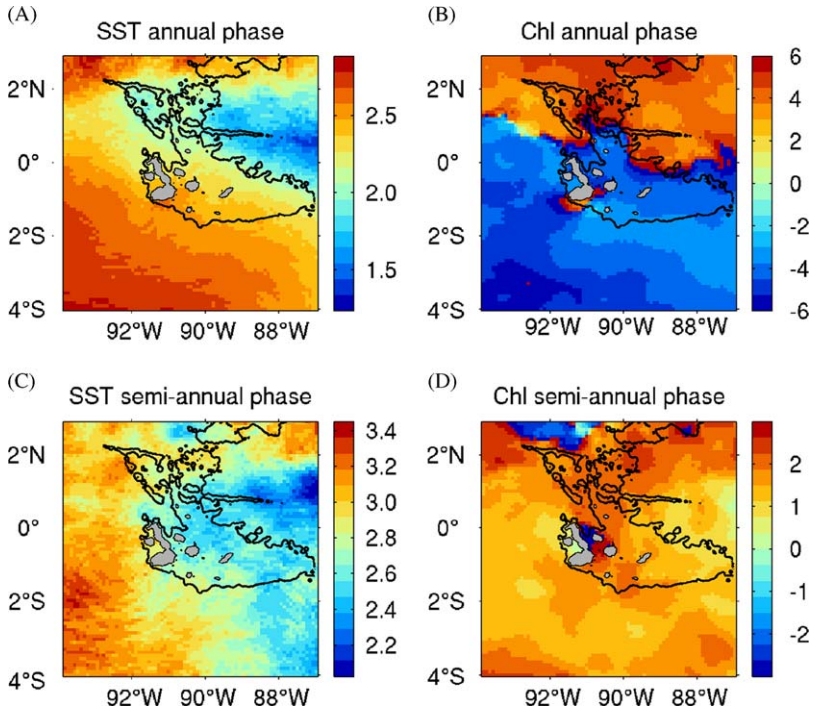

Fig. 5. Harmonic analysis: (A,B) annual phase constituents for SST and ocean color, respectively (both in months relative to January); and (C,D) semi-annual phase constituents for the same variables (both in months relative to January). Black contour indicates the 2000-m isobath.

transition between the two regimes is abrupt and takes place along a meandering band between 1°N and 2°N that roughly corresponds with the location of the EF.

Although the semi-annual amplitude constituents for both SST and chl were only important in localized areas, the semi-annual phases depict large-scale patterns (Figs. 5C and D). This constituent has been associated with the westward propagation of the seasonal cycle along the equator (Lukas, 1986; Yu and McPhaden, 1999), and with other intraseasonal phenomena (e.g. Kelvin waves) that are not well resolved by monthly climatologies.

5. Empirical orthogonal function analysis

A conventional empirical orthogonal function (EOF) analysis (Emery and Thomson, 1997), which decomposes the temporal variance at each spatial location after removing the time-averaged mean, yielded the annual and semi-annual components of the seasonal cycle in the first two modes, and it did not provide any new information. Specifically, none of the dominant modes were associated with the local effects of the EUC, which have been described as a quasi-permanent pool of cold water on the western side of Isabela and Fernandina islands (Houvenaghel, 1978). Alternatively, EOFs can be computed after removing the spatial mean at each time step (Lagerloef and Bernstein, 1988). In this case, the EOFs decompose the variability of the spatial property gradients rather than the variability of the property itself (Kelly, 1988). These "spatial variance EOFs", also called "gradient EOFs" (Paden et al., 1991), are useful when the purpose is to investigate the variance associated with features that do not vary strongly over time (Lagerloef and Bernstein, 1988).

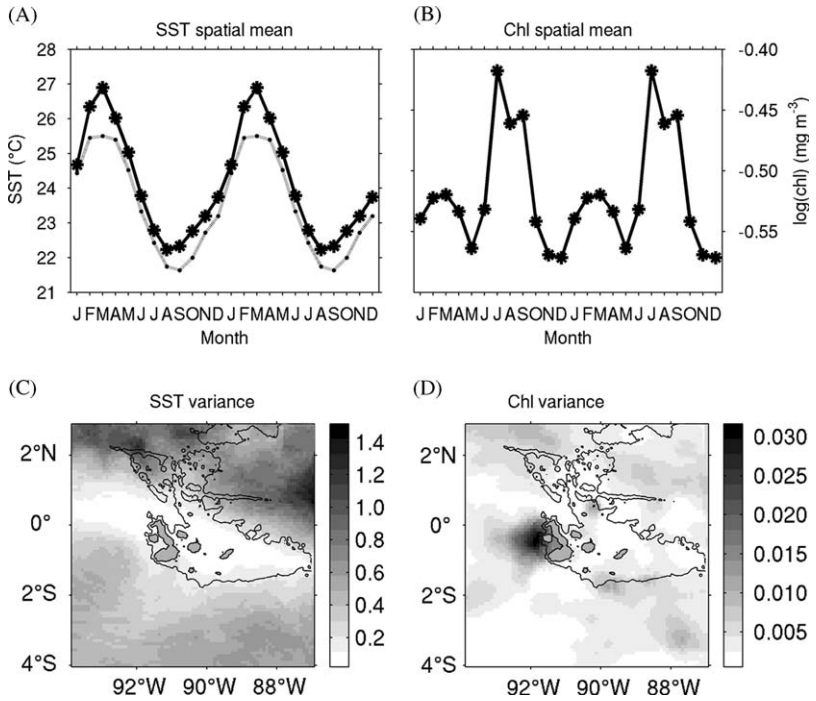

Fig. 6. EOF analysis: (A,B) monthly spatial means for SST and log-transformed chl, respectively, that were removed from the time series prior to the EOF analysis; and (C,D) temporal variance decomposed by the analysis for SST ($^{\circ}C^2$) and log-transformed chl [$(mg\,m^{-3})^2$], respectively. Black contour indicates the 2000-m isobath. Time series are repeated twice for clarity. Dashed line in (A) is the long-term (1965–2001) monthly averaged SST measured at the CDRS dock. The location of the CDRS dock is indicated in Fig. 2.

The spatial means that were removed at each time step following this method are shown in Fig. 6. Both averages exhibit a clear seasonality, with a maximum SST in March of 26.9°C and a minimum in August of 22.2°C (Fig. 6A). The chl time series depicts a semi-annual cycle with the first peak occurring in March ($0.3\,mg\,m^{-3}$) and a second, larger peak occurring between July and September ($0.4\,mg\,m^{-3}$) (Fig. 6B). The variance fields of the adjusted data matrices (i.e. that variance which is decomposed by the gradient EOF analysis) are shown in Fig. 6C and D for SST and chl, respectively.

The dominant mode in the SST EOF decomposition explains 92.2% of the variance of the adjusted monthly climatologies. Its spatial pattern (Fig. 7A) is similar to the temporal mean described at the beginning of Section 4 (Fig. 3A). There is a strong north–south temperature gradient, with the zero crossing corresponding with the southern boundary of the EF. A large pool of cooler-than-average water extends west of Islabela and Fernandina islands. The first gradient EOF mode for the chl data explains 82.9% of the variance. Although a large-scale north–south gradient is also evident, the main feature is a concentric pattern of above-average chl centered in Elizabeth Bay, the southern of two bodies of water formed between Isabela and Fernandina islands (Fig. 7B).

Gradient mode 2 captures 6% of the SST spatial variability. Its spatial pattern exhibits a zonal band of cool water between 2°N and 2°S, with a large pool of cold water on the eastern side of the archipelago and a smaller pool directly west of Isabela and Fernandina islands (Fig. 7C). Warmer-than-average waters are found along the northern and southern edges of the study area. For the chl decomposition, the second mode describes 7.7% of the variance. Above-average chl concentrations are found occupying the

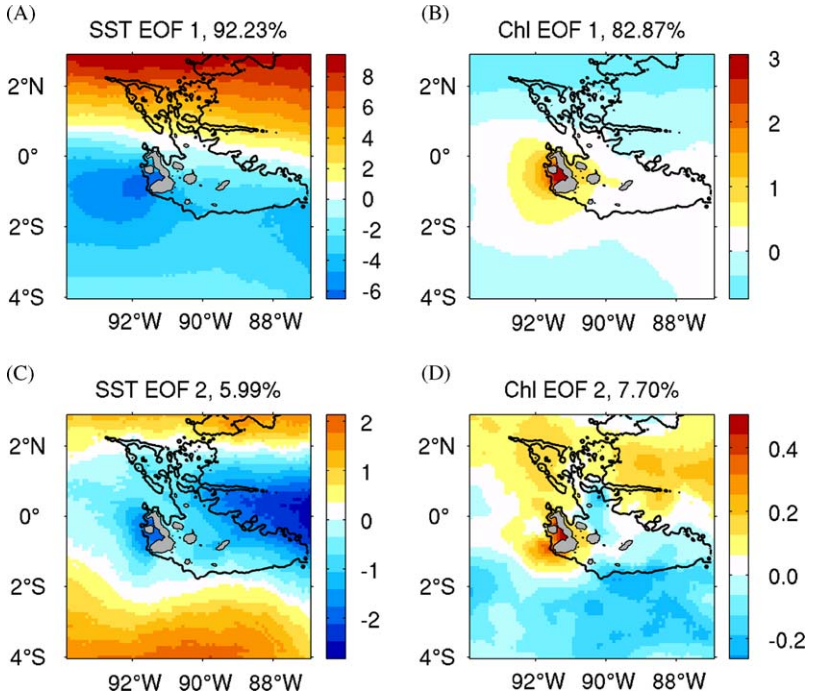

Fig. 7. EOF analysis: (A,B) mode 1 spatial patterns for SST and log-transformed chl, respectively; and (C,D) mode 2 spatial patterns for the same variables. Black contour indicates the 2000-m isobath.

northern half of the study area, and a distinct center of high chl is again found in Elizabeth Bay (Fig. 7D). Below-average chl concentrations are found along the southern sector.

The temporal amplitudes associated with each EOF are presented in Fig. 8. The mode 1 amplitudes are positive for the SST, and consist of an annual cycle with a minimum in March and a maximum in September (Fig. 8A). Thus, the spatial pattern is well developed during the second half of the year, and its timing is consistent with the intensification of generalized wind-driven equatorial upwelling south of the EF (Fig. 7A). The linearity of the spatial pattern along east–west bands is suggestive of persistent zonal flows most likely associated in the South Equatorial Current (SEC; Fig. 1), which is strong between July and December (Johnson et al., 2002). The extent and axis of orientation of the cold pool off Isabela and Fernandina are also consistent with westward advection of upwelled EUC waters by the SEC.

Mode 1 temporal amplitudes for chl describe a positive cycle with two peaks of similar magnitude during the year; the first one in January and the second one in August. Chl levels are low between February and July and somewhat higher between September and December (Fig. 8B). This suggests that the local response by phytoplankton to the annual cold tongue cycle and the intensification of the SEC is complex and also may be influenced by nutrient availability. The spatial pattern associated with this mode (Fig. 7B) is only strong in the waters surrounding the western group of islands, and to a lesser degree in a zonal band extending roughly between 1°N and 3°S. These waters are probably under the enriching influence of the EUC, as will be discussed in the next section.

The temporal amplitudes of the SST mode 2 depict an annual cycle with positive values between January and July (peaking in April) and negative values between August and December (minimum in October) (Fig. 8C). The

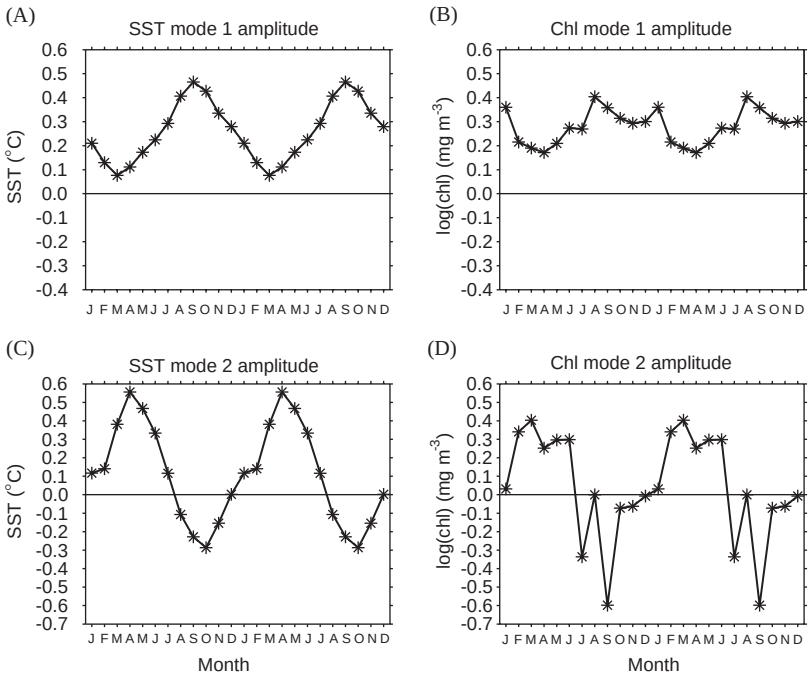

Fig. 8. EOF analysis: (A,B) mode 1 temporal amplitudes for SST and log-transformed chl, respectively; and (C,D) mode 2 temporal amplitudes for the same variables. Time series are repeated twice for clarity.

corresponding spatial pattern (Fig. 7C) is thus most intensified in April, and its timing is consistent with the strengthening and shoaling of the EUC in the eastern Pacific (Lukas, 1986; Johnson et al., 2002). The pool of cold water on the western side of Fernandina and Isabela during this time represents EUC waters forced to surface by the steep slopes of these islands. Colder-than-average waters also surround the central and northern group of islands. The large cold pool impinging on the eastern side of the archipelago is consistent with the influx of upwelled waters from the Panamá Bight, which also occurs between December and April (Cromwell and Bennett, 1959; Wooster, 1959).

Chl mode 2 temporal amplitudes (Fig. 8D) are also positive between January and June (but they peak in March, a month earlier than the SST time series), and generally negative between July and December (the minimum occurs in September). As expected, high chl values occupy the same general area where the cool waters are found, although a slight shift to the north is apparent in the chl field (Fig. 7D).

It is argued that the gradient EOFs picked up patterns consistent with surface manifestations of the EUC and its seasonality in the second mode. The small percentage of the variance represented by this mode (about 6% for SST and 8% for chl) is attributed to two factors. First, it should be borne in mind that the satellite sensors (especially the AVHRR) measure surface properties that respond primarily to the tightly coupled ocean–atmosphere system of the eastern equatorial Pacific (i.e, the meridional migration of the trade wind belts and the associated ITCZ). Thus, the cooling effect of a strong and shallow EUC during the austral fall is attenuated by warming at the surface. Independent evidence of this effect is present in the long-term monthly average of a 37-year (1965–2001) in situ SST time series (dashed line in Fig. 6A) measured daily at the dock of the Charles Darwin Research Station (CDRS in Fig. 2), on Santa Cruz Island. Although rapid

warming occurs between December and February, the curve flattens out in March, revealing the slight cooling influence of the EUC at a time when the region as a whole reaches maximum temperatures (i.e. the solid line in Fig. 6A). Podestá and Glynn (1997) have actually documented a dip of a few tenths of a degree in March in an annual cycle estimated from a seasonal-trend decomposition of the daily values in the CDRS time series (see also Fig. 1 in Abbott (1966) for a similar behavior in a time series at Wreck Bay, San Cristóbal Island). The smaller peak in the chl spatial mean (Fig. 6B) during March is also consistent with EUC enhancement at this time.

A second reason has to do with the use of climatological time series composed of only 12 monthly steps. The variance contained in these data is small compared to that in the original time series used to construct them. In addition, such time series tend to be dominated by the seasonal cycle, while intraseasonal and interannual variability are de-emphasized or lost.

The SST and chl amplitude time series do not always overlap. This may be in part due to the fact that the climatologies were derived from different base periods (1985–1997 for SST and 1996–2003 for ocean color), that large interannual signals (i.e. El Niño/La Niña) may have biased the data in different ways, and that the chl signal is inherently noisier than the smooth SST. Also, the ocean-color sensor measures chl concentrations within the first optical attenuation depth (i.e. the upper 5–25 m of the water column), while the SST measurement is limited to the skin (i.e. the top 1 mm) of the water column, so that the ocean-color sensor may in fact detect changes in the water column before the SST sensor does.

In spite of these caveats, it should be noted that the contribution of mode 2 to the variability in the data sets is not always small. The reconstructed time series for this mode, obtained by multiplying the values in the spatial pattern at each location by the temporal amplitudes, can at times have a greater magnitude than the reconstructed time series for the dominant mode. This can be visualized online in Animations 2 and 3. For example, during March and April the reconstructed SST time series for mode 2 is greater than the time series for mode 1 by up to 0.85°C in the coldest areas. Therefore, mode 2 or, rather, the SST and chl gradients induced by the processes described above, can be important during the fall months.

6. Water-column temperature and nitrate

Because satellite measurements are restricted to the surface or, at best, to the upper tens of meters of the water column, further understanding of the processes that drive the observed SST and chl patterns can be gained by considering the vertical distribution of temperature and the role of nutrient availability. Monthly values of water-column temperature and quarterly values of nitrate concentration at 20 m were extracted from the World Ocean Atlas 1998 (WOA98) (Conkright et al., 1998). The WOA98 is compiled by the National Oceanographic Data Center (NODC) of the National Oceanic and Atmospheric Administration (NOAA), and it contains objectively analyzed property fields for 1° squares and standard depth levels.

Meridional sections of temperature in the upper 150 m along 92.5°W (west of the Galápagos Platform) and 87.5°W (east of the Galápagos Platform) for March and September (Fig. 9) were chosen to represent conditions at the seasonal extremes of the annual cycles identified in the previous sections. The main feature in the western sections is the upward sloping of the isotherms associated with the local upwelling of the EUC between 0°S and 1°S, as it impinges against the island platform and is deflected upward. In the eastern sections, past the influence of the archipelago, the presence of a shallow EUC is evident by the upward and downward bulging of the isotherms roughly between 10 and 100 m. Seasonally, maximum SSTs are reached in March and the water column is strongly stratified during this month (Figs. 9A and B). By September the southern part of the study area has been dramatically changed. The warm upper layer (~30 m) has been eroded by the southeast trade winds, and these waters have been replaced by

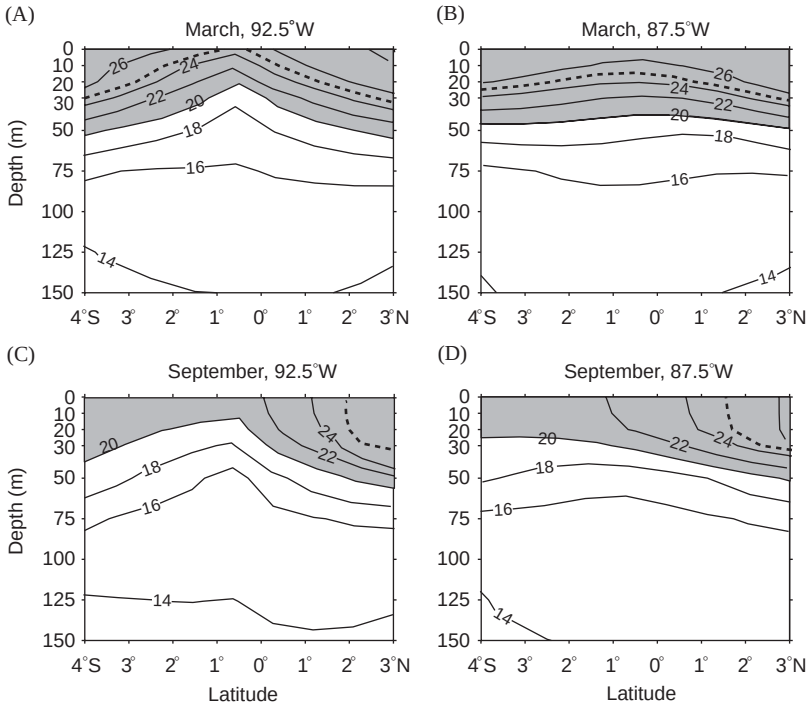

Fig. 9. WOA98 meridional temperature (°C) sections: (A,B) for March along 92.5°W (west of the archipelago) and 87.5°W (east of the archipelago), respectively; and (C,D) for September. Temperatures $\geqslant 20$°C are shaded, and the 25°C isotherm is dashed.

cool, upwelled water from the top of the thermocline (Figs. 9C and D). The EF, indicated by the 25°C isotherm at the surface just south of 2°N (the dashed line in Figs. 9C and D), separates warm and stratified waters to the north from mixed waters to the south. The surface divergence created by the wind stress at this time is also conducive to enhanced upwelling of the EUC (Fig. 9C), as evidenced by the steep sloping of the isotherms all the way down to the bottom of the thermocline ($\sim$100 m).

Horizontal distributions of WOA98 nitrate concentration at 20 m (Fig. 10) for the four quarterly periods illustrate the seasonal progression of macronutrients reaching the upper layer. During the January–March period (Fig. 10A), and away from the area of influence of the EUC (i.e. in the stratified regime), nitrate concentrations are relatively low ($\leqslant 6\,\mu$M), implying a mesotrophic to oligotrophic character. Elevated nitrate concentrations expand and propagate along the southern half of the study area from east to west during the rest of the year (Figs. 10B–D), as the southeast trade winds and the equatorial upwelling intensify. An opposite trend is evident along the northern half, such that oligotrophic and HNLC regimes coexist in the study area during the second part of the year. Minimum 20-m nitrate concentrations can be as low as 0.2 μM north of the EF while maximum concentrations can reach 15 μM in the southwest sector of the study area in the October–December period (Fig. 10D).

South of the EF, nitrate levels are adequate to support large phytoplankton populations year-round. Yet, elevated chl levels are primarily observed in association with the pool of cold water on the western side of Isabela and Fernandina islands, where the EUC upwells. The IronEx I and II experiments (Martin et al., 1994; Coale et al., 1996b; Coale, 1998) demonstrated that low ambient iron concentrations limit the ability of phytoplankton populations to fully utilize

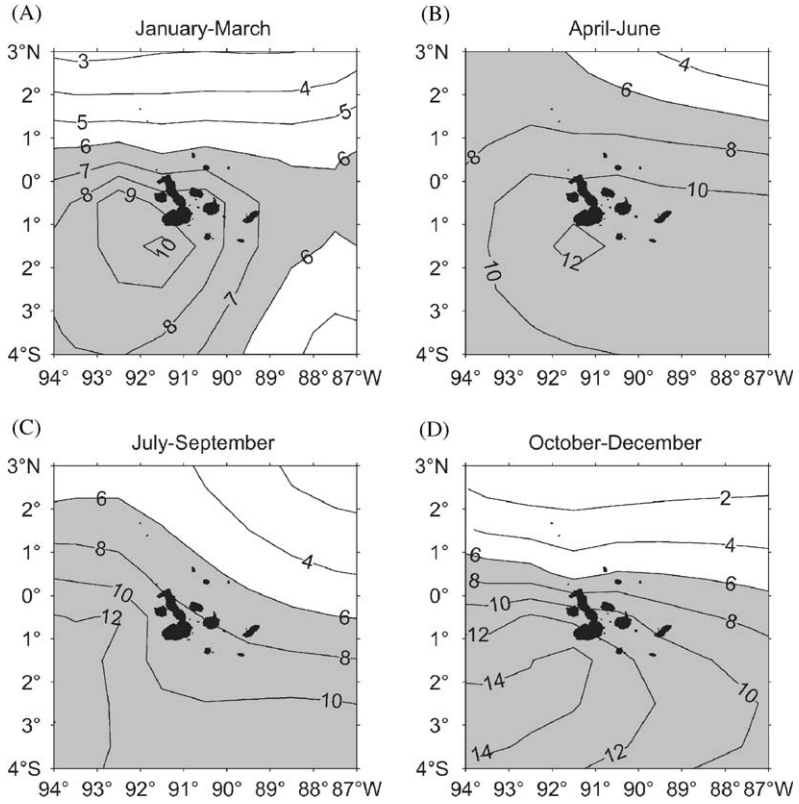

Fig. 10. WOA98 nitrate concentrations (μM) at 20 m: (A) for January–March; (B) for April–June; (C) for July–September; and (D) for October–December. $[NO_3] \geqslant 6\,\mu M$ are shaded.

available nitrate and achieve maximal growth in this region. While the EUC contains somewhat enhanced concentrations of iron (up to 0.35 nM at 140°W) (Coale et al., 1996a), water from the EUC alone cannot explain the high chl levels observed at the upwelling site. A dramatic enrichment of this water takes place by contact with the island platform, accounting for iron concentrations >1 nM (up to 3 nM were measured in Bolivar Channel between Isabela and Fernandina during IronEx I) (Martin et al., 1994; Gordon et al., 1998). As the iron limitation is relieved in the Bolivar Channel and Elizabeth Bay, phytoplankton production increases by several fold (Lindley and Barber, 1998) while nitrate levels are locally depleted (Chavez and Brusca, 1991; Sakamoto et al., 1998).

7. Summary and conclusion

Harmonic analysis of satellite-derived SST and ocean-color monthly climatologies around the Galápagos Islands showed that the temporal variability was dominated by a basin-wide seasonal cycle of warming and cooling of surface waters (and its effect on phytoplankton), associated with the north–south migration of the ITCZ. The two annual cycles described by the first two modes of the gradient EOF analysis were consistent with the seasonalities of the SEC and the EUC, respectively, suggesting that these modes captured some of the effects of these currents as they interact with the archipelago. An influx of Panamá Bight waters in the eastern side of the archipelago was also consitent with

the results of these analyses. In addition, several of the observed patterns showed a slight tilt aligned with the east–west axis of the Galápagos Platform, suggesting that the presence of the archipelago may modify the large-scale fields by partially deflecting westward flows originating from South America (e.g. SEC, Panamá Bight Influence).

The satellite data were useful in delineating the seasonal behavior of the quasi-permanent pool of cold water and high chl formed by the upwelling of the EUC on the western side of the archipelago. Elizabeth Bay was identified as the area where the phytoplankton response is most dramatic and persistent, due to a localized source of iron from the island platform, which relieves the limitation for this micronutrient and allows the phytoplankton to fully use the available macronutrients.

The identification of distinct annual cycles of phytoplankton abundance in both the harmonic and EOF analyses of the ocean-color climatologies is in contrast with previous studies, which had failed to demonstrate a clear chl seasonality (Harris, 1969; Houvenaghel, 1978, 1984; Kogelschatz et al., 1985; Feldman, 1986). This is not surprising, however, considering that the two annual cycles identified here have opposing schedules, making it difficult to discern seasonal patterns in a time series without more sophisticated analyses.

Finally, it is noted that most of the effects described in this paper would be missed or greatly attenuated if the analyses had been carried out on a larger scale or at a coarser resolution. However, they have clearly played an important role in the establishment and evolution of the unique biota found in the nearshore environments of the archipelago (e.g. Abbott, 1966; Glynn et al., 1983). From this perspective, the results of this paper provide a descriptive framework relevant to marine ecological and biogeographic studies of the islands. With the recently established 14,000,000-hectare "Galápagos Marine Reserve" (Bensted-Smith, 1998), these results may also be useful for purposes of zonation and management, particularly of the offshore waters.

Acknowledgements

On-line data sets were obtained from the following sources. The "Pathfinder + Erosion" SST climatologies from PO.DAAC/JPL/NASA (URL: http://podaac.jpl.nasa.gov/order/order_sstemp.html#Product112). SIMBIOS-NASDA-OCTS and SeaWiFS ocean color from the SeaWiFS project (code 970.2) and the GES DISC DAAC (code 902) at GSFC/ NASA, Greenbelt, MD 20771 (URLs: http://daac.gsfc.nasa.gov/data/dataset/OCTS/ and http://daac.gsfc.nasa.gov/data/dataset/SEAWIFS/). The "Smith and Sandwell" global sea-floor topography V. 8.2 (for Figs. 4–7) from the Institute of Geophysics and Planetary Physics at the Scripps Institution of Oceanography (URL: http://topex.ucsd.edu/marine_topo/mar_topo.html). WOA98 temperature and nitrate from NODC/NOAA (URL: http://www.nodc.noaa.gov/). The 37-year (1965–2001) in situ SST record from Academy Bay was graciously provided by S. Rea of the Monitoring Program at the CDRS. K.S. Casey (NODC/NOAA), provided computer code useful in generating the ocean-color climatologies. This study was supported by the Endowed Marine Mammal Program at Oregon State University. Insightful discussions with E. Beier, D.B. Chelton, and A.M. Martinez on analysis techniques were helpful. This manuscript benefited from comments from B.R. Mate, C.B. Miller, P.T. Strub, and A. Thomas.

References

Abbott, D.P., 1966. Factors influencing the zoogeographic affinities of the Galápagos inshore marine fauna. In: Bowman, R.I. (Ed.), The Galápagos: Proceedings of the Symposia of the Galápagos International Scientific Project. University of California Press, Berkeley, pp. 108–122.

Anderson, J.J., 1977. Identification and tracing of water masses with an application near the Galápagos Islands. Ph.D. Thesis, University of Washington, Seattle, Washington, Unpublished, 144pp.

Bensted-Smith, R., 1998. The special law for Galápagos. Noticias de Galápagos 59, 6.

Casey, K.S., Cornillon, P., 1999. A comparison of satellite and in situ-based sea surface temperature climatologies. Journal of Climate 12 (6), 1848–1863.

Chavez, F.P., Brusca, R.C., 1991. The Galápagos Islands and their relation to oceanographic processes in the tropical Pacific. In: James, M.J. (Ed.), Galápagos Marine Invertebrates. Taxonomy, Biogeography, and Evolution in Darwin's Islands. Topics in Geobiology, Vol. 8. Plenum Press, New York and London, pp. 9–33, 474pp.

Coale, K.H. (Ed.), 1998. The Galápagos iron experiments: a tribute to John Martin. Deep-Sea Research II 45, 915–1150.

Coale, K.H., Fitzwater, S.E., Gordon, R.M., Johnson, K.S., Barber, R.T., 1996a. Control of community growth and export production by upwelled iron in the equatorial Pacific. Nature 379, 621–624.

Coale, K.H., Johnson, K.S., Fitzwater, S.E., Gordon, R.M., Tanner, S., Chavez, F.P., Ferioli, L., Sakamoto, C., Rogers, P., Millero, F., Steinberg, P., Nightingale, P., Cooper, D., Cochlan, W.P., Landry, M.R., Constantinou, J., Rollwagen, G., Trasvina, A., Kudela, R., 1996b. A massive phytoplankton bloom induced by an ecosystem-scale iron fertilization experiment in the equatorial Pacific Ocean. Nature 383, 495–501.

Conkright, M., Levitus, S., O'Brien, T., Boyer, T., Antonov, J., Stephens, C., 1998. World Ocean Atlas 1998 CD-ROM data set documentation. Technical Report 15, NODC Internal Report, Silver Spring, MD, 16pp.

Cromwell, T., Bennett, E.B., 1959. Surface drift charts for the eastern tropical Pacific Ocean. Inter-American Tropical Tuna Commission Bulletin 3 (5), 217–237.

Delcroix, T., 1993. Seasonal and interannual variability of sea surface temperatures in the tropical Pacific, 1969–1991. Deep-Sea Research I 40 (11–12), 2217–2228.

Emery, W.J., Thomson, R.E., 1997. Data Analysis Methods in Physical Oceanography. Pergamon Press, Exeter, UK, 634pp.

Feldman, G.C., 1986. Patterns of phytoplankton production around the Galápagos Islands. In: Bowman, M.J., Yentsch, C.M., Peterson, W.T. (Eds.), Tidal Mixing and Plankton Dynamics. Lecture Notes on Coastal and Estuarine Studies, Vol. 17. Springer, Berlin, pp. 77–106.

Feldman, G., Clark, D., Halpern, D., 1984. Satellite color observations of the phytoplankton distribution in the eastern equatorial Pacific during the 1982–1983 El Niño. Science 226 (4678), 1069–1071.

Glynn, P.W., Wellington, G.M., Wells, J.W., 1983. Corals and Coral Reefs of the Galápagos Islands. University of California Press, Berkeley, 330pp.

Gordon, R.M., Johnson, K.S., Coale, K.H., 1998. The behaviour of iron and other trace elements during the IronEx-I and PlumEx experiments in the equatorial Pacific. Deep-Sea Research II 45, 995–1041.

Harris, M.P., 1969. Breeding seasons of sea-birds in the Galápagos Islands. Journal of Zoology, London 159, 145–165.

Hayes, S.P., 1985. Sea level and near surface temperature variability at the Galápagos Islands, 1979–83. In: Robinson, G., del Pino, E.M. (Eds.), El Niño in the Galápagos Islands: The 1982–1983 Event. Publication of the Charles Darwin Research Foundation for the Galápagos Islands. Quito, Ecuador, pp. 49–81.

Houvenaghel, G.T., 1978. Oceanographic conditions in the Galápagos Archipelago and their relationships with life on the islands. In: Boje, R., Tomczak, M. (Eds.), Upwelling Ecosystems. Springer, Berlin, pp. 181–200.

Houvenaghel, G.T., 1984. Oceanographic setting of the Galápagos Islands. In: Perry, R. (Ed.), Key Environments, Galápagos. Pergamon Press, Oxford, pp. 43–54.

Johnson, G.C, Sloyan, B.M., Kessler, W.S., McTaggart, K.E., 2002. Direct measurements of upper ocean currents and water properties across the tropical Pacific during the 1990s. Progress in Oceanography 52 (1), 31–61.

Kelly, K.A., 1988. Comment on "Empirical orthogonal function analysis of advanced very high resolution radiometer surface temperature patterns in Santa Barbara Channel" by G.S.E. Lagerloef and R.L. Bernstein. Journal of Geophysical Research 93, 15753–15754.

Kogelschatz, J., Solorzano, L., Barber, R., Mendoza, P., 1985. Oceanographic conditions in the Galápagos Islands during the 1982/1983 El Niño. In: Robinson, G., del Pino, E.M. (Eds.), El Niño in the Galápagos Islands: The 1982–1983 Event. Publication of the Charles Darwin Research Foundation for the Galápagos Islands. Quito, Ecuador, pp. 91–123.

Lagerloef, G.S.E., Bernstein, R.L., 1988. Empirical orthogonal function analysis of advanced very high resolution radiometer surface temperature patterns in Santa Barbara Channel. Journal of Geophysical Research 93 (C6), 6863–6873.

Lindley, S.T., Barber, R.T., 1998. Phytoplankton response to natural and experimental iron addition. Deep-Sea Research II 45 (6), 1135–1150.

Lukas, R., 1986. The termination of the Equatorial Undercurrent in the eastern Pacific. Progress in Oceanography 16, 63–90.

Martin, J.H., Coale, K.H., Johnson, K.S., Fitzwater, S.E., Gordon, R.M., Tanner, S.J., Hunter, C.N., Elrod, V.A., Nowicki, J.L., Coley, T.L., Barber, R.T., Lindley, S., Watson, A.J., Van Scoy, K., Law, C.S., Liddicoat, M.I., Ling, R., Stanton, T., Stockel, J., Collins, C., Anderson, A., Bidigare, R., Ondrusek, M., Latasa, M., Millero, F.J., Lee, K., Yao, W., Zhang, J.Z., Friederich, G., Sakamoto, C., Chavez, F., Buck, K., Kolber, Z., Greene, R., Falkowski, P., Chisholm, S.W., Hoge, F., Swift, R., Yungel, J., Turner, S., Nightingale, P., Hatton, A., Liss, P., Tindale, N.W., 1994. Testing the iron hypothesis in ecosystems of the equatorial Pacific Ocean. Nature 371, 123–129.

Paden, C.A., Abbott, M.R., Winant, C.D., 1991. Tidal and atmospheric forcing of the upper ocean in the Gulf of California 1. Sea surface temperature variability. Journal of Geophysical Research 96 (C10), 18337–18359.

Pak, H., Zaneveld, J.R.V., 1973. The Cromwell Current on the east side of the Galápagos Islands. Journal of Geophysical Research 78 (33), 7845–7859.

Palacios, D.M., 2002. Factors influencing the island-mass effect of the Galápagos Islands. Geophysical Research Letters 29 (23), 2134 (doi: 10.1029/2002GL016232).

Podestá, G.P., Glynn, P.W., 1997. Sea surface temperature variability in Panamá and Galápagos: extreme temperatures causing coral bleaching. Journal of Geophysical Research 102 (C7), 15749–15759.

Sakamoto, C.M., Millero, F.J., Yao, W., Friederich, G.E., Chavez, F.P., 1998. Surface seawater distributions of inorganic carbon and nutrients around the Galápagos Islands: results from the PlumEx experiment using automated chemical mapping. Deep-Sea Research II 45, 1055–1071.

Strub, P.T., Mesías, J.M., Montecino, V., Rutllant, J., Salinas, S., 1998. Coastal ocean circulation off western South America. In: Robinson, A.R., Brink, K.H. (Eds.), The Sea, Ideas and Observations on Progress in the Study of the Seas, Vol. 11, Global Coastal Ocean Regional Studies and Syntheses. Wiley, New York, pp. 273–313.

Wooster, W.S., 1959. Oceanographic observations in the Panama Bight, ''Askoy'' Expedition, 1941. Bulletin of the American Museum of Natural History 118, 113–152.

Yu, X., McPhaden, M.J., 1999. Seasonal variability in the equatorial Pacific. Journal of Physical Oceanography 29, 925–947.